AMERICAN SOCIETY FOR MICROBIOLOGY | mBio®

RESEARCH ARTICLE

The Human Disease-Associated Aβ Amyloid Core Sequence Forms Functional Amyloids in a Fungal Adhesin

Rachele D. Rameau,[a,b] Desmond N. Jackson,[a,b] Audrey Beaussart,[c]* Yves F. Dufrêne,[c] Peter N. Lipke[a,b]

Biology Department, Brooklyn College, City University of New York, Brooklyn, New York, USA[a]; Biology PhD Program, The Graduate Center, City University of New York, New York, New York, USA[b]; Institute of Life Sciences, Université Catholique de Louvain, Louvain-la-Neuve, Belgium[c]

* Present address: Laboratoire Interdisciplinaire des Environnements Continentaux (LIEC) CNRS, Université de Lorraine, UMR 7360, Vandoeuvre-lès-Nancy, F-54501, France.

R.D.R. and D.N.J. contributed equally to this work.

ABSTRACT **There is increasing evidence that many amyloids in living cells have physiological functions. On the surfaces of fungal cells, amyloid core sequences in adhesins can aggregate into 100- to 1,000-nm-wide patches to form high-avidity adhesion nanodomains on the cell surface. The nanodomains form through interactions that have amyloid-like properties: binding of amyloid dyes, perturbation by antiamyloid agents, and interaction with homologous sequences. To test whether these functional interactions are mediated by typical amyloid interactions, we substituted an amyloid core sequence, LVFFA, from human Aβ protein for the native sequence IVIVA in the 1,419-residue *Candida albicans* adhesin Als5p. The chimeric protein formed cell surface nanodomains and mediated cellular aggregation. The native sequence and chimeric adhesins responded similarly to the amyloid dye thioflavin T and to amyloid perturbants. However, unlike the native protein, the nanodomains formed by the chimeric protein were not force activated and formed less-robust aggregates under flow. These results showed the similarity of amyloid interactions in the amyloid core sequences of native Als5p and Aβ, but they also highlighted emergent properties of the native sequence. Also, a peptide composed of the Aβ amyloid sequence flanked by amino acids from the adhesin formed two-dimensional sheets with sizes similar to the cell surface patches of the adhesins. These results inform an initial model for the structure of fungal cell surface amyloid nanodomains.**

IMPORTANCE **Protein amyloid aggregates are markers of neurodegenerative diseases such as Alzheimer's and Parkinsonism. Nevertheless, there are also functional amyloids, including biofilm-associated amyloids in bacteria and fungi. In fungi, glycoprotein adhesins aggregate into cell surface patches through amyloid-like interactions, and the adhesin clustering strengthens cell-cell binding. These fungal surface amyloid nanodomains mediate biofilm persistence under flow, and they also moderate host inflammatory responses in fungal infections. To determine whether the amyloid-like properties of fungal surface nanodomains are sequence specific, we ask whether a disease-associated amyloid core sequence has properties equivalent to those of the native sequence in a fungal adhesin. A chimeric adhesin with an amyloid sequence from the Alzheimer's disease protein Aβ instead of its native sequence effectively clustered the adhesins on the cell surface, but it showed a different response to hydrodynamic shear. These results begin an analysis of the sequence dependence for newly discovered activities for fungal surface amyloid nanodomains.**

Received 20 October 2015 **Accepted** 2 December 2015 **Published** 12 January 2016

Citation Rameau RD, Jackson DN, Beaussart A, Dufrêne YF, Lipke PN. 2016. The human disease-associated Aβ amyloid core sequence forms functional amyloids in a fungal adhesin. mBio 7(1):e01815-15. doi:10.1128/mBio.01815-15.

Editor Antonio Cassone, University of Perugia

Address correspondence to Peter N. Lipke, plipke@brooklyn.cuny.edu.

This article is a direct contribution from a Fellow of the American Academy of Microbiology.

Amyloids are ordered insoluble protein aggregates and important functional components of many processes and are now known to exist in all domains of life (1–6). Amyloids are characterized by "cross-β" structures in which amyloid core sequences consisting of 4 to 7 amino acids form β-strands that are assembled into β-sheets that can include thousands of these short strands arranged side by side. The β-strands are perpendicular to the long dimension of the β-sheet. The sheets can stack to form long fibrils characteristic of amyloid structures (7, 8). Although amyloid fibers and deposits are best known in neurodegenerative diseases and serum deposits, it is now clear that some amyloid assemblies have functional characteristics as well (9–13). Among the functional amyloids, the Pmel-derived fibrils within mammalian melanosomes, for example, are assembled through amyloid interactions to form a template for melanin deposition (11). Bacterial functional amyloids are key components in biofilms of both Gram-positive and Gram-negative organisms (12, 14–17). In fungi, amyloid-like prions have both pathogenic and beneficial features, and they can mediate epigenetic regulation of gene expression and generate transcriptional diversity in clonal populations of yeast cells (4, 18, 19). Amyloid interactions mediate assembly of fungal spore coats, which are highly refractory to

detrimental environmental conditions (20, 21). Additionally, fungal adhesins contain functional amyloid-forming regions that mediate robust fungal aggregation and biofilm formation (5, 22, 23). In this system, application of force unfolds protein domains to expose amyloid-forming core sequences. As a result, the adhesins aggregate in patches on the cell surface (5, 13, 23), and the presence of the surface patches is associated with a reduced host inflammatory response to fungal infections in *Caenorhabditis elegans* and in abscesses in human autopsy sections (24–27).

In *Candida albicans*, the *ALS* gene family encodes cell surface adhesins with a common architecture: an N-terminal secretion signal sequence, a globular ligand-binding region with two Ig-like invasin domains, a conserved T domain (now also called AFR [for amyloid-forming region] [28, 29]), and a set of tandem repeats (TR) that mediate hydrophobic effect interactions. A 600- to 1,000-residue Ser/Thr-rich glycosylated stalk provides a flexible linker. The C-terminal region is covalently bonded to cell wall glucans through a modified glycosylphosphatidylinositol (GPI) anchor (29–32).

Each T domain/AFR of Als proteins contains a conserved amyloid-forming core sequence, which forms amyloid fibers in solution. However, these fibers cannot form *in vivo*, because the proteins are physically constrained by their anchorage on the cell wall. Nevertheless, the amyloid core sequences mediate formation of cell surface patches of arrayed adhesin molecules ("adhesin nanodomains"). The nanodomains are 100- to 1,000-nm-wide patches containing hundreds to thousands of adhesin molecules, and therefore, they bind to multivalent ligands with high avidity. Nanodomain formation is inhibited by antiamyloid drugs and does not occur if the amyloid core sequence of the agglutinin is mutated to a nonamyloid sequence (22, 23, 33). These observations are consistent with nanodomain formation through amyloid-like interaction of the amino acids in the amyloid core sequence.

Als surface nanodomains form in response to moderate extension force applied to the adhesins: force can unfold the T domain/AFR, facilitating amyloid nanodomain formation (22, 34). Such unfolding can result from forces of 50 to 100 pN per molecule applied by atomic force microscopy (AFM) or under laminar flow at moderate shear stress ($\geq$0.5 dyne $\cdot$ cm^{-2}). The amyloid nanodomains also form during fungal aggregation assays, as cells and ligand-coated beads exert forces on each other as they are mixed at moderate speed. The resulting nanodomains are very high-avidity binding sites and lead to creation of large cellular aggregates and greatly strengthened biofilms (5, 23, 35, 36).

T domains/AFRs of the *C. albicans* adhesins Als1p, Als3p, and Als5p contain a core amyloid sequence I^{325}VIVA^{329}. A single amino acid change, V326N, greatly reduces the potential to form amyloids, and leads to reduced surface nanodomains and attenuated biofilm formation (5, 22, 23, 36).

Given that functional amyloids play ever-expanding roles in cell adhesion and other aspects of biology, we questioned whether the specific sequence in Als proteins is essential and whether a nonhomologous amyloid core sequence would be equivalent. Specifically, we ask whether a disease-associated amyloid sequence has equivalent structural properties and whether it would mediate nanodomain formation and strengthened adhesion. Therefore, we investigated the effect of substituting the amyloid sequence IVIVA of Als5p by the LVFFA fragment of human Aβ amyloid core sequence, which is well characterized as a component of amyloids *in vitro* (8, 37–39). The two peptides show similar β-aggregation potential, >90%, in the predictor TANGO (40) and have similar aggregation propensities in AGGRESCAN (41). The functional consequences of this substitution allow us to determine the specificity of action of each amyloid sequence, as well as provide data for our first models for the structure of cell surface amyloid nanodomains.

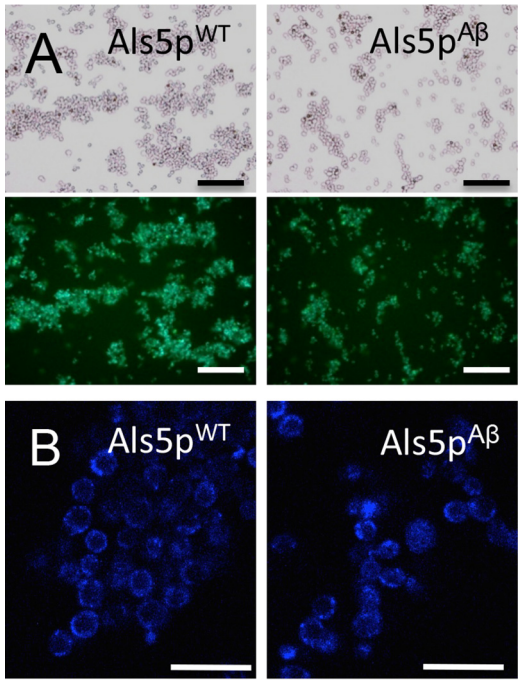

FIG 1 Aggregation activity and thioflavin T staining of cells expressing Als5p. (A) Cells expressing Als5p^{WT} or Als5p$^{A\beta}$ were aggregated with BSA-coated beads (dark spheres) in the presence of ThT (300 nM). Phase-contrast micrographs are above the corresponding fluorescence images. Bars = 20 μm. (B) Confocal images of ThT-stained cells expressing Als5p^{WT} and Als5p$^{A\beta}$. Bars = 10 μm.

RESULTS

Expression. We substituted the Aβ amyloid core sequence LVFFA for the natural Als5p core sequence IVIVA at positions 325 to 329 of the 1,419-residue protein in the *Saccharomyces cerevisiae* expression plasmid pJL1. This construct also encodes a V5 epitope tag immediately following the secretion signal sequence (23). When the modified construct (designated pJL1-Als5p$^{A\beta}$) was transformed into *S. cerevisiae*, Als5p$^{A\beta}$ was expressed on the cell surface. Immunofluorescence with a fluorescein-conjugated antibody to the V5 epitope showed that surface expression of Als5p$^{A\beta}$ was comparable to that of the native sequence protein Als5p (designated Als5p^{WT} [WT stands for wild type]; see Fig. S1 in the supplemental material).

Activity and amyloid properties of Als5p$^{A\beta}$. Like native Als5p^{WT}, the Als5p$^{A\beta}$ chimera mediated both adhesion to bovine serum albumin (BSA)-coated beads and fungal cell-cell aggregation (Fig. 1A). However, cells expressing Als5p$^{A\beta}$ formed smaller aggregates. Quantitative assays showed the level of adhesion to be about 50% that of Als5p^{WT} (Fig. 1A and 2). Although Als5p^{WT} is activated by vortex mixing of the cells expressing Als5p^{WT}, the Als5p$^{A\beta}$ chimera was not affected by this treatment (see Fig. S2 in the supplemental material) (35).

We tested whether Als5p$^{A\beta}$ formed thioflavin T (ThT) fluores-

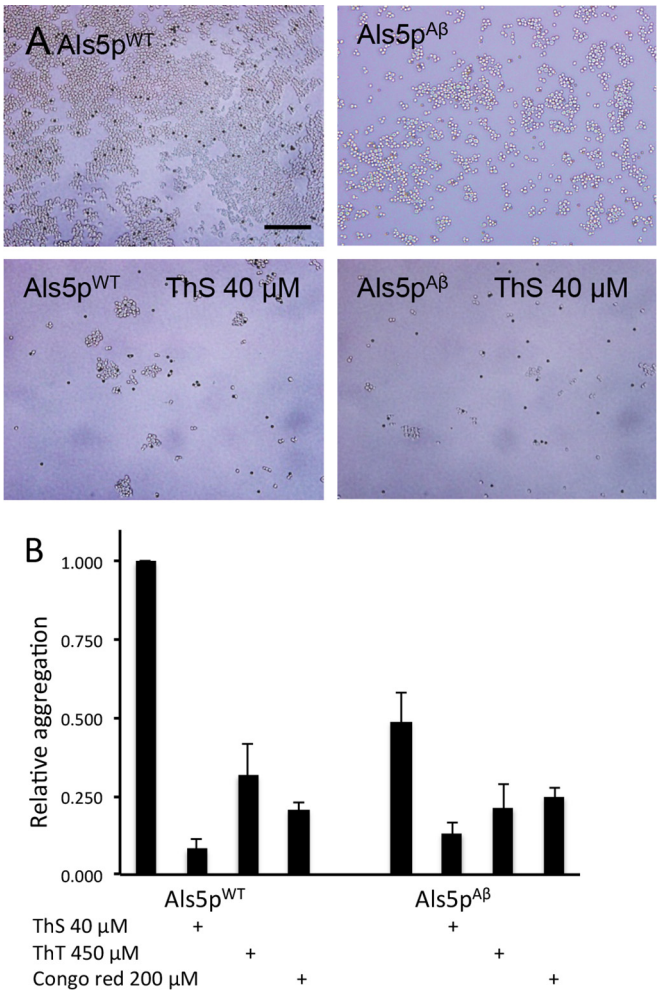

FIG 2 Effects of amyloid inhibitors on cell aggregation. Cells expressing Als5p^{WT} or Als5p$^{A\beta}$ were aggregated with beads coated with denatured BSA in the absence or presence of amyloid inhibitors. (A) Qualitative effect of thioflavin S (ThS) (40 μM). Bar = 20 μm. (B) Quantitative assays. Values are means plus standard errors of the means (SEM) (error bars) for three experiments.

cent nanodomains. Figure 1A shows that surfaces of cells expressing Als5p$^{A\beta}$ were effectively stained with ThT at 300 nM, similar to cells expressing Als5p^{WT}. At this concentration, ThT does not inhibit activity of Als5p (23). Cells expressing Als5p$^{A\beta}$, like cells expressing Als5p^{WT}, showed surface ThT-bright puncta characteristic of amyloid nanodomains (22, 23) (Fig. 1B).

To determine whether adhesion of cells expressing Als5$^{A\beta}$ showed amyloid properties, we carried out assays in the presence of inhibitory concentrations of the amyloid-perturbing dyes ThT, thioflavin S (ThS), or Congo red (CR). These dyes inhibited cell adhesion and aggregation, with similar sensitivities for Als5p^{WT} and Als5p$^{A\beta}$ (Fig. 2). ThS was more effective as an inhibitor than ThT, as we have previously observed (35, 42, 43). In contrast, the dyes do not affect adhesion or aggregation of cells expressing the nonamyloid Als5p^{V326N}, which is significantly less active (23). Therefore, the LVFFA core sequence from Aβ, like the wild-type Als5p core sequence, mediated nanodomain formation and enhanced activity of Als5p in an amyloid-like fashion.

Because amyloids consist of repeating arrays of identical sequences, they can be perturbed by peptides of similar sequence (44, 45). Als5p amyloid interactions are enhanced by treatment with a homologous amyloid-forming peptide and are inhibited by a mutated peptide (23, 27). Accordingly, we assessed the effects of such peptides for Als5p$^{A\beta}$ activity and nanodomain formation. The chimeric peptide SNGLVFFATTRTV incorporates the Aβ amyloid core sequence flanked on each end by the three flanking residues of the native core. This chimeric peptide at 14 μM enhanced aggregation in cells expressing Als5p$^{A\beta}$ (Fig. 3A and B). Conversely, the single-site substitution peptide SNGINIVATTRTV (substituted amino acid underlined) is an effective inhibitor of aggregation in Als5p (Fig. 3D) (23), but it was ineffective as an inhibitor of Als5p$^{A\beta}$ (Fig. 3C). Therefore, Als5p$^{A\beta}$ bound a peptide with homologous sequence but did not respond to an inhibitory peptide based on the native amyloid core sequence from Als5p^{WT} (Fig. 3C).

When the chimeric peptide was suspended in deionized water, it formed ribbon-like structures with straight edges (Fig. 3E). The ribbons were up to 3 μm long, with widths up to 300 nm. The ribbon structures were similar to tapes and planar structures recently reported for other peptides with amyloid core sequences (38, 39). Some of the structures in the chimeric peptide sample showed fiber-like images, as if the ribbons were folded or associated along the long axis.

Single-molecule force analysis of Als5p$^{A\beta}$. We analyzed the response to force of Als5p$^{A\beta}$ on cell surfaces. Under mechanical force, Als5p^{WT} molecules *in situ* show successive unfolding of specific domains: first the amyloid core containing the T domain, then the tandem hydrophobic repeats, and finally the Ig-invasin domains. This molecular stretching in turn triggers clustering of the adhesins on the cell surface.

Single-molecule atomic force microscopy (AFM) was used to map the domain unfolding and spatial distribution of individual Als5p$^{A\beta}$ on live cells using AFM tips functionalized with anti-V5 antibodies (22, 36, 46). Yeast cells expressing V5-tagged proteins were immobilized into porous polymer membranes (Fig. 4D, inset). Figure 4A and B show an adhesion force histogram and representative force-distance curves, recorded between the antibody-tip and the surfaces of different yeast cells. A substantial proportion (21%) of force curves showed adhesion signatures reflecting the detection of single Als5p$^{A\beta}$ proteins. Two types of force signatures were observed, i.e., low-adhesion force curves (Fig. 4B, bottom curves) with single small adhesion forces, and high-adhesion force curves (Fig. 4B, top curves) showing sawtooth patterns with multiple large force peaks. These complex curves show successive unfolding of individual domains of Als5p$^{A\beta}$ (36). The detection frequency, 21%, corresponded to a minimum protein surface density of ~215 proteins/μm^2, similar to that for Als5p^{WT} (22).

Interestingly, the maps (Fig. 4D) revealed that most proteins formed clusters about 100 to 350 nm in size, resembling the domains reported for Als5p^{WT} on force-activated *ALS5*-expressing *S. cerevisiae* cells (22). In analyses of Als5p^{WT}, such clusters formed 12 to 90 min after Als5p molecules had been pulled with the AFM tip. A single site mutation in the amyloid-forming sequence of the protein demonstrated that the amyloid core sequence I^{325}VIVA is required for clustering; thus, the nanodomains depend on amyloid interactions. The similarity of results with Als5p$^{A\beta}$ leads us to believe that the clusters observed here result from amyloid-like bonds between Aβ core sequences. However, in the present study,

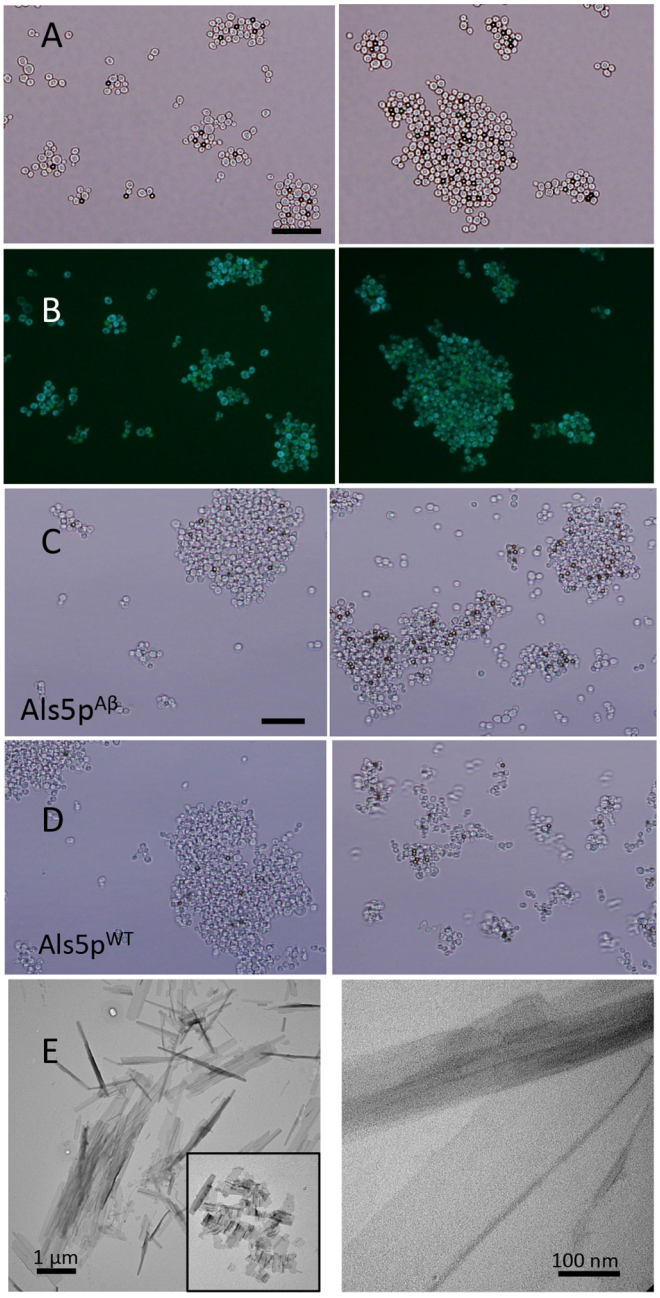

FIG 3 Amyloid sequence peptides. (A) Effect of chimeric peptide on aggregation of Als5p$^{A\beta}$ cells. (Left) Aggregation without peptide; (right) aggregation in the presence of chimeric peptide SNGLVFFATTRTV (20 μg/ml). Bar = 10 μm. (B) Fluorescence images of fields in panel A stained with ThT (300 nM). (C) Effects of Als5p antiamyloid peptide on aggregation of Als5p$^{A\beta}$. (Left) Cells without added peptide; (right) aggregation in the presence of SNGINIVATTRTV (200 μg/ml). Bar = 10 μm. (D) Effects of antiamyloid peptide on cells expressing Als5p^{WT}. (Left) Aggregation without added peptide; (right) aggregation in the presence of SNGINIVATTRTV (200 μg/ml). The images are at the same magnification as in panel C. (E) Transmission electron micrographs of negative-stained structures of peptide SNGLVFFATTRTV at low (left) and high (right) magnification. The large pictures are from a sample gently shaken. (Inset) Nanodomain-sized structures from a stirred sample. The image in the inset is at the same magnification as the large image.

clustering did not require preactivation by mechanical force. Unlike Als5p^{WT}, there was no increase in clustering when Als5p$^{A\beta}$ cells were probed a second time. This could mean that maximal clustering occurs even without mechanical stimuli or that the cells were already preactivated because they were more sensitive to small shear forces associated with cell preparation (35).

In unfolding curves (Fig. 4B and C), the maximal rupture forces were similar for Als5p^{WT} and Als5p$^{A\beta}$; however, the mean distance to rupture was longer for the Als5p$^{A\beta}$ chimeric protein: 287.1 ± 7.4 nm versus 253.3 ± 17.9 nm for Als5p^{WT} (mean ± standard error [SE]; n = 15). Inspection of the force-distance curves showed that the difference was in the extension length in the region corresponding to the T domains/AFRs, which are the first to unfold (marked with blue and red arrows in Fig. 4C) (36). Specifically, the extended region between these arrows shows that the T domain/AFR unfolds with very little or no additional application of force to form a longer segment.

Force effects and catch bonding in Als5p$^{A\beta}$. In cells expressing As5p^{WT}, amyloid nanodomains are formed under laminar flow or during vortex mixing (35, 42). We therefore compared the cells under laminar flow. Cells expressing Als5p^{WT}, Als5p$^{A\beta}$, or the nonamyloid substitution mutant Als5p^{V326N} were forced to flow through a Bioflux laminar flow device, the surface of which was coated with denatured BSA, an Als5p ligand. Shear stress was increased in steps over a range from 0.02 to 20 dynes · cm^{-2}. Time lapse videomicroscopy recorded the cells as they flowed through the imaging window in the laminar flow device. We analyzed two parameters: the fraction of the substrate area covered in adhered cells, and the mean size of the aggregates.

Three forms of Als5p mediated differences in adhesion to substrate and cell-cell aggregation under flow. As expected, cells expressing the nonamyloid mutant Als5p^{V326N} bound only at low shear rates, apparently reflecting weak interactions with the surface (Fig. 5, red curves) (42). There were few aggregates formed, and the largest aggregates bound only at the lowest shear rates. For Als5p^{V326N}, the mean aggregate area was ~300 pixel units. Most adhering cells were washed off at a shear stress of 0.8 dyne · cm^{-2}, and all cells were washed off at 2 dyne · cm^{-2} or greater.

In contrast, cells with Als5p^{WT} adhered poorly to substrate at the lowest shear stresses (0.02 and 0.2 dyne · cm^{-2}), with poor coverage and only small aggregates present (Fig. 5, blue curves). At shear stresses of 0.8 to 5 dynes · cm^{-2}, there was good binding to substrate, and large aggregates were present, with mean aggregate areas 4- to 5-fold greater than for the nonamyloid Als5p^{V326N} (Fig. 5B). Large aggregates stuck to the surface and persisted, especially after the shear stress was increased to 0.8 dyne · cm^{-2}, 2.0 dyne · cm^{-2}, and 5.0 dyne · cm^{-2}. Most cells were dislodged by shear stress of 10 dyne · cm^{-2}, and all cells were washed off at 20 dyne · cm^{-2}, stresses 10-fold greater than needed to dislodge Als5p^{V326N} cells.

Cells expressing Als5p$^{A\beta}$ had very different adhesion and aggregation behavior (Fig. 5, green curves). There was successively greater binding as shear stress increased from low to moderate levels, then a decrease at shear stresses above 5 dynes · cm^{-2}. The adhesion increased gradually as the shear stress increased, rather than showing a threshold effect as in Als5p^{WT} (Fig. 5A). Single cells and aggregates of 2 to 5 cells flowed through the imaging window, then some stuck to the substrate or to preexisting aggregates. In general, cells expressing Als5p$^{A\beta}$ covered more of the visualized field, but the aggregates were more numerous and

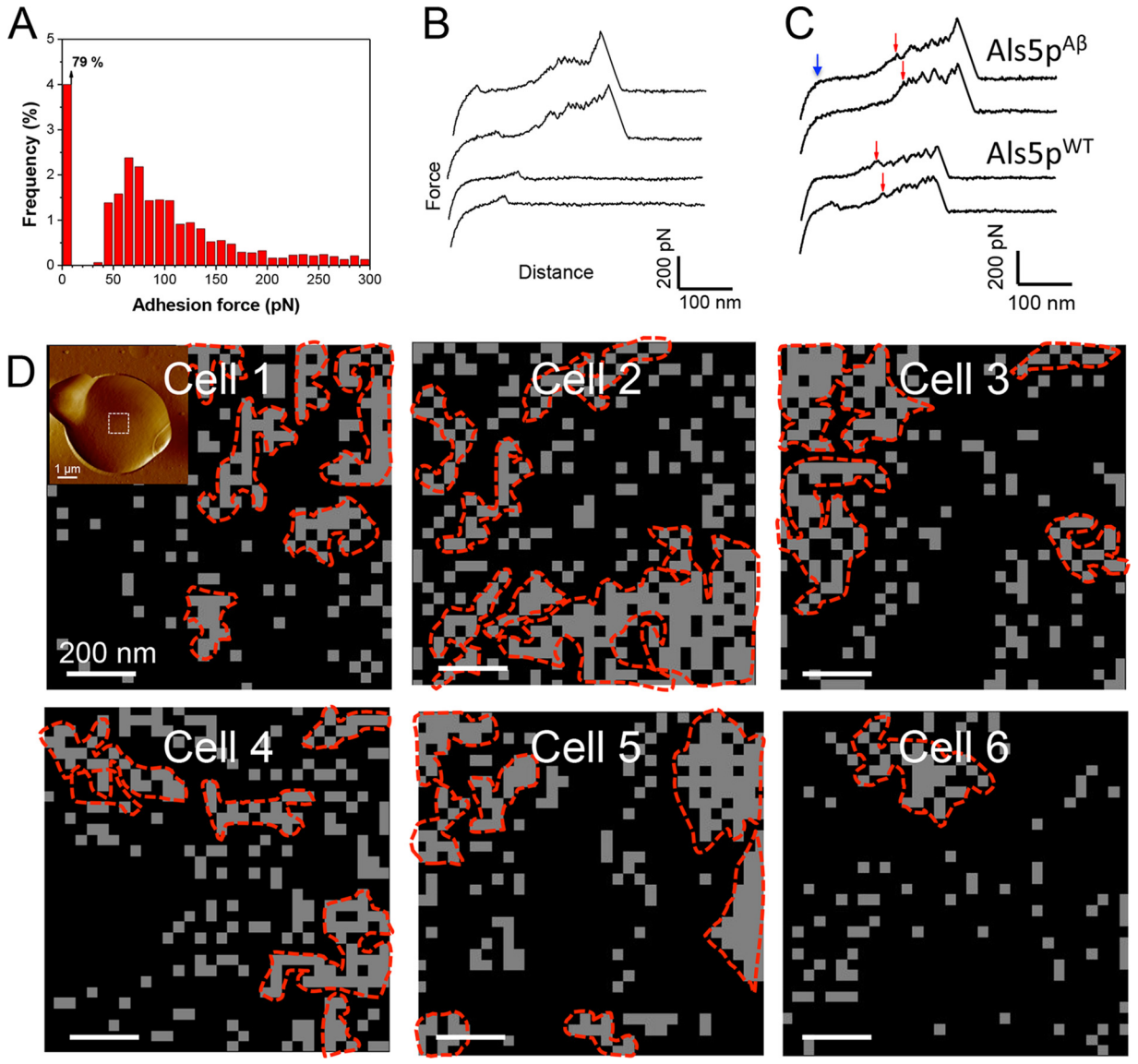

FIG 4 Single-molecule imaging of Als5p$^{A\beta}$ proteins on yeast cells. (A) Adhesion force histogram ($n = 6{,}144$ curves) from six Als5p$^{A\beta}$-expressing cells obtained in buffer between anti-V5 functionalized tips (different cultures and different tips). (B) Representative force-distance curves highlighting dual detection: single weak adhesion peaks reflecting Als epitope recognition (bottom curves) and sawtooth patterns with multiple force peaks documenting Als5p Ig-to-ligand multipoint binding, followed by the unfolding of the entire protein (top curves). (C) Comparison of representative force-distance curves for Als5p$^{A\beta}$ and Als5p^{WT}. Note the different lengths between the red and blue arrows, which delimit the region corresponding to T-domain unfolding. (D) Adhesion force maps (1 μm × 1 μm) recorded in buffer with anti-V5 tips on six Als5p$^{A\beta}$-expressing cells. The heterogeneous distribution of gray pixels, which each represent the detection of single Als5p proteins, documents the formation of nanoscale clusters (highlighted by red dashed lines). (Inset) AFM deflection image (5 × 5 μm^2) recorded in buffer, showing an *S. cerevisiae* cell expressing V5-tagged Als5p$^{A\beta}$ proteins, trapped in a porous membrane for AFM analysis.

smaller. The mean aggregate size reached a maximum of 375 pixel units at 2.0 dynes · cm^{-2}, 130% of the maximal aggregate size for cells expressing nonamyloid Als5p^{V326N} (Fig. 5B). These data show that Als5p$^{A\beta}$ mediated catch bonding (strengthening bonds under shear stress), but the cells flowing through the chamber bound incrementally, whereas catch bonding of cells expressing Als5p^{WT} was triggered at a threshold and led to larger aggregates that were more likely to bind or dissociate as mass events.

DISCUSSION

The amyloid core sequence from human Aβ mediated formation of functional amyloid nanodomains in the *C. albicans* adhesin Als5p, when substituted for the Als5p native amyloid core sequence. Like the native sequence protein, Als5p$^{A\beta}$ clustered the adhesin molecules on the cell surface and potentiated cell adhesion. However, differences in the behavior of Als5p^{WT} and Als5p$^{A\beta}$ adhesins under flow highlight the unique characteristics of the native sequence.

Similarities. Als5p^{WT} and Als5p$^{A\beta}$ were similarly localized to the cell wall and mediated formation of surface amyloid nanodomains (Fig. 1, 2, and 4; see Fig. S1 in the supplemental material). Both forms of Als5p mediated adhesion to ligand-coated beads and multicellular aggregation (Fig. 1 and 2). In contrast,

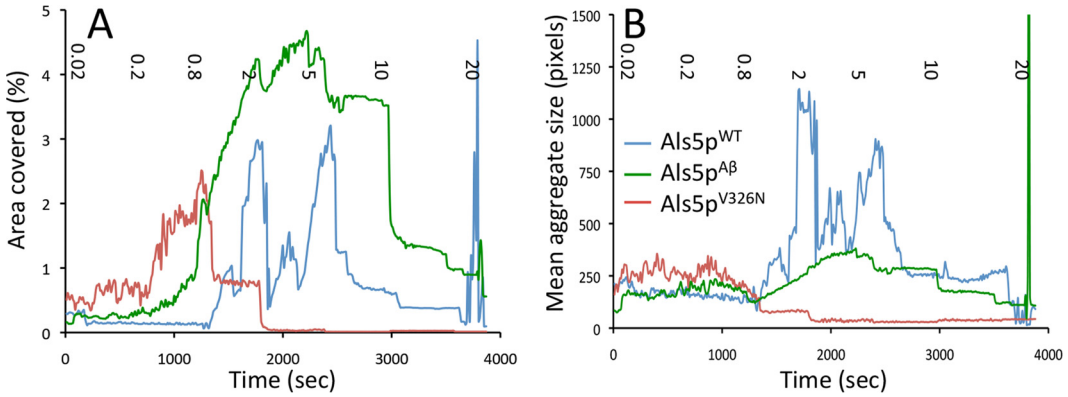

FIG 5 Effects of laminar flow on adhesion of cells expressing Als5p. Cells expressing each of the designated forms of Als5p were forced to flow through a Bioflux 200 laminar flow device and imaged by phase-contrast microscopy at 1-s intervals. The flow rate was increased stepwise in 10-min intervals to generate shear stresses from 0.02 to 20 dyne · cm^{-2}, as denoted at the top of each panel. Each frame was analyzed with ImageJ for the fraction of the field covered by cells (A) and average size of adhering aggregates (B). Mean values for 10-s windows are plotted.

$Als5p^{V326N}$, which contains a sequence that does not form amyloids, is expressed well but does not cluster on the cell surface (22, 23). The clustering in $Als5p^{WT}$ and $Als5p^{A\beta}$ has the characteristics of surface amyloid nanodomains in that the clustered adhesins are highly fluorescent with the amyloid-sensitive dye ThT at a nanomolar concentration (Fig. 1). $Als5p^{WT}$ and $Als5p^{A\beta}$ were also similarly sensitive to inhibition of adhesion activity by micromolar concentrations of amyloid-perturbing dyes Congo red, ThT, and ThS (Fig. 2). These dyes reduced adhesion to the levels observed in cells expressing $Als5p^{V326N}$.

Because protein amyloids are stabilized by side chain interactions between β-strands of identical sequence, peptides with the same sequence can interact to reinforce the amyloids (7, 44). Conversely, mutated sequences can inhibit formation of amyloid arrays. As an example, the tridecapeptide SNGIVIVATTRTV, containing the amyloid core sequence of $Als5p^{WT}$, increases the size of aggregates and ThT fluorescence of amyloid nanodomains, and a mutant nonamyloid peptide (SNGINIVATTRTV) inhibits both fluorescence and aggregation (23). This inhibitory peptide did not affect aggregation caused by $Als5p^{A\beta}$ (Fig. 3C). However, the homologous sequence peptide SNGLVFFATTRTV enhanced amyloid nanodomains and adhesion activity for $Als5p^{A\beta}$ (Fig. 3A). Therefore, $Als5p^{A\beta}$ had characteristics similar to $Als5p^{WT}$ in its ability to form amyloid-like ThT-fluorescent surface nanodomains that bound homologous sequence peptides and potentiated cell adhesion and aggregation.

AFM single-molecule force-distance analysis of cells expressing $Als5p^{A\beta}$ showed cell surface density values similar to $Als5p^{WT}$ (~200 molecules per μm^2 as a minimal estimate) and similar sizes of the surface nanodomains (Fig. 4) (22). Both $Als5p^{A\beta}$ and $Als5p^{WT}$ had two types of force-distance curves, a smooth curve characteristic of weak interactions, and a strong interaction curve with a sawtooth shape characteristic of sequential domain unfolding events (36). The force histograms were similar to those for $Als5p^{WT}$, except that the minimal disruptive force increased from 45 pN to 60 pN (22).

Comparisons of the unfolding lengths and sequence lengths show that the T domain/AFR, containing the amyloid-forming sequence, unfolds first, followed by the six tandem repeats, and finally the Ig-invasin-like domain at the N terminus of the protein (5, 32, 47). Both the force required and the molecular extensions were similar for the regions corresponding to unfolding of the tandem repeats and Ig-invasin domains in both versions of the protein. However, the extension length of the region of the curve corresponding to the T domain/AFR of $Als5p^{A\beta}$ was 42 nm longer than for $Als5p^{WT}$ (Fig. 5B and C) (22, 23). This difference corresponds well with the expected increase in chain length for a fully unfolded T domain (108 residues × 0.36 nm per residue = 38.9 nm). Therefore, this difference would be expected if the T domain/AFR fully unfolds in the Aβ chimeric protein, but not in $Als5p^{WT}$. This difference would be the result if the T region/AFR were destabilized due to changes in packing of the LVFFA sequence within the domain.

Response to laminar flow. The adhesion and aggregation behavior of $Als5p^{A\beta}$ under flow was significantly different from that of the native sequence protein. Binding of $Als5p^{WT}$ to ligand-coated beads leads to activation of the entire yeast cell surface to an adhesive state that mediates extensive cell-cell aggregation (29, 30). This activation is caused by formation and propagation of amyloid nanodomains, following a protein remodeling event (34). Application of force initiates this transition, because extension in the AFM, laminar flow over the cells, or vortex mixing triggers nanodomain formation and activation of adhesion (22, 23, 35, 42). Specifically, exposure to a laminar flow shear stress of $\geq$0.5 dyne · cm^{-2} or vortex mixing at 2,500 rpm for 1 min activates the adhesin (35, 42). In contrast to $Als5p^{WT}$, $Als5p^{A\beta}$ was clustered initially in AFM mapping experiments (Fig. 4); clustering was not increased in subsequent maps and was not further activated by vortex mixing (see Fig. S2 in the supplemental material) (22, 23). Under laminar flow, $Als5p^{A\beta}$ showed gradually increasing adhesion and higher probability of binding as the shear stress was raised. In contrast, $Als5p^{WT}$ showed a strong activation threshold and adhesion of much larger aggregates (Fig. 5). Together, this evidence supports the ideas that, like $Als5p^{WT}$, $Als5p^{A\beta}$ mediates formation of adhesin nanodomains on the cell surface, and can also mediate catch bonds (bonds that strengthen under tension). However, the adhesin with the Aβ sequence was not activated by extension force and did not show the characteristics expected if activity were dependent on protein refolding.

A model for amyloid nanodomains. The chimeric peptide SNGLVFFATTRTV showed a propensity to form planar structures, rather than amyloid fibers (Fig. 3E). These structures are

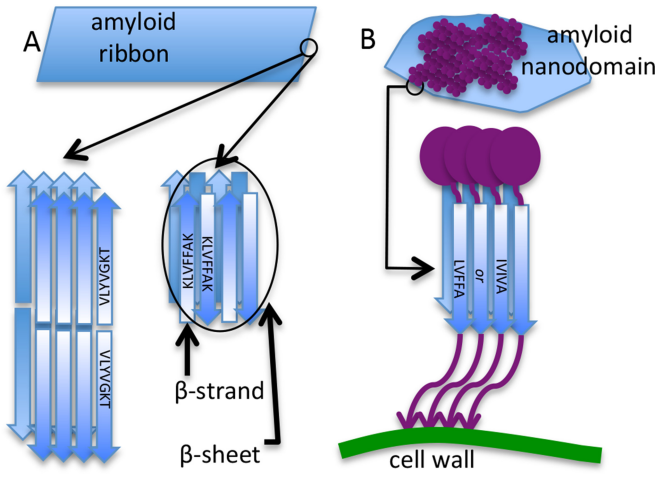

FIG 6 Planar amyloid-like assemblies. (A) Amyloid ribbon. Two proposed structures are shown, looking from the short edge of the ribbon. β-Strands are viewed looking down on side chains, so the interstrand hydrogen bonds would be horizontal in the plane of the image, and β-sheets are depicted as being planar with the image. Both structures show β-sheets stacked face-to-back, so the same face is visible on each sheet. (Left) Bilayer parallel sheet structure proposed by Morris et al. (39). (Right) Antiparallel structure proposed by Dai et al. (38). (B) Possible nanodomain structure formed by Als5p. (Top) View looking face on at a cell surface. (Bottom) Model for amyloid-like interactions viewed from an edge of the nanodomain. β-Strands of IVIVA (Als5p^{WT}) or LVFFA (Als5p^{Aβ}) make parallel β-sheets, stacked face to back as in panel A. N-terminal Ig-like invasin domains (5, 48) are shown as purple ovals, and the C-terminal stalks are shown as purple arrows connected covalently to cell wall glucans (green) (31, 32).

like those in recent models for aggregates of some amyloid sequence peptides. Molecular ribbons made from a peptide containing the α-synuclein core sequence, VLYVGSKT, can be up to 400 to 500 nm wide, about the size of the largest nanodomains for Als5p (39). The structure is consistent with a bilayer of amyloid sheets, with hydrophobic N-terminal portions of the peptide sequestered in the interior and C-terminal hydrophilic residues exposed to the aqueous solvent (Fig. 6A). Similar amyloid ribbons assemble from the Aβ-derived peptide KLVFFAK in an amyloid monolayer with both ends of the peptide exposed to the solvent (38). In each structure, the β-strands are perpendicular to the plane of the ribbon. These structures have in common the fact that they are composed of identical β-strands forming β-sheets with minimal twist. The sheets are stacked front to back through steric zipper interactions of the side chains (8, 38, 39). Therefore, all interactions between the sheets are equivalent, and additional β-sheets can add to the structure with equivalent binding energy. In the α-synuclein-derived sequence, all strands are parallel, corresponding to class 2 amyloids (8). The Aβ-derived sheets are composed of antiparallel β-sheets, corresponding to class 6 amyloids.

Fungal adhesins have properties consistent with similar formation of two-dimensional amyloid-like patches on the cell surface. Because adhesin C termini are anchored to the cell wall, the orientation of the potential β-strands is probably parallel, with the C-terminal region of the amyloid sequences proximal to the cell, and N-terminal regions distal (Fig. 6B). The β-sheets might then be stacked front to back, with steric zipper interactions mediating sheet-to-sheet associations, a class 2-like structure. Such nanodomains could grow by adding β-strands to the edges of the sheets or by adding sheets to the stack. Therefore, geometric properties of the observed nanodomains are compatible with the structures of amyloid ribbons, rather than fibers. In support of this idea, our data show that in the context of the Als5p protein sequence, the Aβ amyloid core sequence LVFFA can form surface nanodomains (Fig. 1B and 4D). Similarly, a chimeric peptide formed sheets with dimensions similar to the nanodomains (Fig. 3E, inset). Thus, the chimeric peptide formed a structure similar to the peptide models (38, 39).

A structural basis for differences between Als5p^{WT} and Als5p^{Aβ}? These differences between Als5p^{WT} and Als5p^{Aβ} may be due to differences in the structure of the T domain/AFR, which contains the amyloid core sequence. Specifically, the T domain/AFR in Als5p^{WT} has characteristics of a well-folded structure that masks the amyloid core sequence until it is unfolded by AFM or shear forces (5, 22, 23, 28, 34, 36). After this unfolding, the amyloid core interacts with core sequences from other Als5p molecules to form amyloid nanodomains (5, 22, 23). The data for Als5p^{Aβ} are consistent with a T domain that is constitutively unstructured: we observed preformed nanodomains in AFM mapping and ThT fluorescence, as well as a more-extended T domain/AFR. Furthermore, unlike Als5p^{WT}, Als5p^{Aβ} showed no additional activation of adhesion activity or nanodomain formation after increased shear by vortex mixing the cells. Thus, the T domain appears to be folded in Als5p^{WT} and constitutively unfolded in Als5p^{Aβ}. Als5p^{Aβ} was less effective than Als5p^{WT} in its cellular aggregation activity (Fig. 2, 3, and 5), consistently generating smaller aggregates. In laminar flow, there was smoother increase in catch bonding and dissociation at high shear stress ("slip bonding"), accompanied by frequent aggregation and dissociation of individual cells in the video frames (not shown). In contrast, binding and dissociation of cells expressing Als5^{WT} usually showed large aggregates being bound or dislodged, implying that the strength of cell-to-cell bonds was greater.

In summary, an amyloid core sequence from human Aβ mediated the formation of functional adhesin nanodomains on the surfaces of cells expressing the *C. albicans* adhesin Als5p. These nanodomains mediated fungal cell adhesion and aggregation, were similarly perturbed by antiamyloid dyes, and interacted with peptides with sequences identical to the amyloid core sequence. Therefore, Als5p^{WT} amyloid nanodomains can be formed from either the native sequence or the Aβ core sequence. However, the catch bonding characteristics under flow depend on the extensibility of the T domain/AFR that includes the amyloid core. Therefore, the Aβ amyloid core sequence mediated the formation of functional adhesin nanodomains on yeast cell surfaces, but sequence-specific structures led to differences in the resultant cellular behavior.

MATERIALS AND METHODS

Strains and media. We used *Saccharomyces cerevisiae* strain W303-1B for expression of all constructs in the pJL1 vector for V5 epitope-tagged Als5p^{WT}, or the vector without an expressed protein, pJL1-EV (EV stands for empty vector) (23). For all experiments, the cells were grown in complete synthetic medium (CSM) lacking tryptophan and with galactose as the carbon source.

Generation of Als5p^{Aβ}. To generate Als5p^{Aβ}, we inserted a synthetic DNA fragment (Integrated DNA Technologies, Coralville, IA) into the SphI-AleI segment of Als5p, using standard molecular biology techniques. The synthetic fragment included a V5 epitope tag, and the Aβ amyloid core sequence LVFFA at positions 325 to 329 replacing the nat-

ural sequence in plasmid pJL1-Als5 using standard molecular techniques. The final construct was verified by restriction analysis and DNA sequencing. The encoded protein was designated Als5p$^{A\beta}$.

Aggregation assays. Aggregation assays were carried out by published methods. Briefly, 10^8 cells in 1 ml of Tris-EDTA (TE) buffer, pH 7.0, were mixed with 10^6 magnetic Dynabeads coated with heat-denatured BSA according to the manufacturer's directions (Invitrogen). The suspension was incubated at 170 rpm at 24°C for 45 min. The tubes were then placed over a magnet to separate the bead-bound cells from the unbound cells, and unbound cells were removed with a Pasteur pipette. The aggregates were washed once with 500 μl of TE buffer and gently resuspended with 100 μl of TE buffer for microscopic observation. Bound cells were quantified by light scattering in a spectrophotometer after dissociation with 1 M NaOH (29, 35).

Fluorescence. To detect the surface expression level of Als5p^{WT} and Als5p$^{A\beta}$, we used fluorescein-conjugated anti-V5 from Life Technologies at a titer of 1:250. Thioflavin T (ThT) staining was carried out as previously described, using 300 nM ThT added in the dark at the beginning of aggregation.

Activation under shear flow. Adhesion and aggregation were tested under laminar flow in a Bioflux 200 laminar flow device and filmed on an Olympus inverted microscope. The chamber was coated with heat-denatured bovine serum albumin, 1 mg · ml^{-1} in TE buffer. Cells suspended in the same buffer (1.2×10^6 cells · ml^{-1}) were forced to flow into the visualization chamber at 0.02 dyne/cm^2, a shear stress that does not activate binding (42). The cells were then imaged at 1-s intervals for 10 min at successive shear stress values of 0.02, 0.2, 0.8, 2, 5, 10, and 20 dynes/cm^2. Images were analyzed with ImageJ.

Peptides. The native sequence peptide SNGIVIVATTRTV, corresponding to sequence positions 322 to 335 in Als5p^{WT}, the nonamyloid peptide SNGINIVATTRTV, and the Aβ sequence peptide SNGLVFFATTRTV were purchased from GenScript. The peptides were dissolved in dimethyl sulfoxide (DMSO).

Transmission electron microscopy. The peptide SNGLVFFATTRTV was suspended in deionized water at 1.9 mg/ml and incubated at 4°C for 2 weeks with gentle shaking on a rotating platform at 60 rpm. A second sample was constantly mixed with a rotating stir bar in a small vial. The resulting materials were adsorbed to Formvar-coated grids, negative stained with uranyl acetate, and imaged on an FEI-Morgagni transmission electron microscope.

AFM measurements. AFM measurements were performed at room temperature in sodium acetate buffer using a Nanoscope VIII Multimode AFM (Bruker, Santa Barbara, CA). Cells were immobilized by mechanical trapping into porous polycarbonate membranes (Millipore), with a pore size similar to the cell size. After filtering a concentrated cell suspension, the filter was gently rinsed with buffer, carefully cut (1×1 cm), and attached to a steel sample puck using double-sided tape, and the mounted sample was transferred into the AFM liquid cell while avoiding dewetting. Cells were first localized using oxide-sharpened microfabricated Si_3N_4 cantilevers (MSCT; Bruker Corporation), and the tip was replaced with a functionalized tip (see below). Adhesion maps on live cells were obtained by recording 32×32 force-distance curves on the area of a given size at the cell surface, calculating the adhesion force at rupture for each force curve, and displaying the value as a gray pixel. All force measurements were recorded with a contact time of 100 ms, an approach and retraction speed of 1,000 nm·s^{-1} and a maximum applied force of 250 pN.

AFM tips were functionalized with anti-V5 antibodies (Invitrogen) using polyethylene glycol (PEG)-benzaldehyde linkers by the method of Ebner et al. (46). Briefly, cantilevers were washed with piranha solution, rinsed in MilliQ water, washed with chloroform, placed in a UV ozone cleaner for 15 min, rinsed with ethanol, and dried with N_2. They were then immersed overnight in an ethanolamine solution (3.3 g of ethanolamine in 6 ml of DMSO), washed three times with DMSO and two times with ethanol, and dried with N_2. The ethanolamine-coated cantilevers were immersed for 2 h in a solution prepared by mixing 1 mg acetal-PEG-NHS (*N*-hydroxysuccinimide) dissolved in 0.5 ml chloroform with 10 μl triethylamine, washed with chloroform, and dried with N_2. Cantilevers were further immersed for 10 min in a 1% citric acid solution, washed with MilliQ water, and then covered with a 200-μl droplet of a solution containing anti-V5 (0.2 mg/ml) to which 2 μl of a 1 M $NaCNBH_3$ solution was added. After 50 min, cantilevers were incubated with 5 μl of a 1 M ethanolamine solution to passivate unreacted aldehyde groups and then rinsed with and stored in acetate buffer.

SUPPLEMENTAL MATERIAL

Supplemental material for this article may be found at http://mbio.asm.org/lookup/suppl/doi:10.1128/mBio.01815-15/-/DCSupplemental.

Figure S1, PDF file, 0.6 MB.

Figure S2, PDF file, 0.1 MB.

ACKNOWLEDGMENTS

We thank Cho Chan for help with the laminar flow experiments, Melissa Garcia-Sherman for help with confocal microscopy, Nicolas Biais for help with electron microscopy, and Michael Cohen for image analyses.

FUNDING INFORMATION

HHS | NIH | National Institute of General Medical Sciences (NIGMS) provided funding to Peter N. Lipke under grant number 1R01 GM098616. Fonds De La Recherche Scientifique - FNRS (F.R.S. - FNRS) provided funding to Yves F. Dufrene.

REFERENCES

1. **Fowler DM, Koulov AV, Alory-Jost C, Marks MS, Balch WE, Kelly JW.** 2006. Functional amyloid formation within mammalian tissue. PLoS Biol **4:**e6. http://dx.doi.org/10.1371/journal.pbio.0040006.
2. **Blanco LP, Evans ML, Smith DR, Badtke MP, Chapman MR.** 2012. Diversity, biogenesis and function of microbial amyloids. Trends Microbiol **20:**66–73. http://dx.doi.org/10.1016/j.tim.2011.11.005.
3. **Dueholm MS, Petersen SV, Sonderkaer M, Larsen P, Christiansen G, Hein KL, Enghild JJ, Nielsen JL, Nielsen KL, Nielsen PH, Otzen DE.** 2010. Functional amyloid in Pseudomonas. Mol Microbiol **77:**1009–1020. http://dx.doi.org/10.1111/j.1365-2958.2010.07269.x.
4. **Holmes DL, Lancaster AK, Lindquist S, Halfmann R.** 2013. Heritable remodeling of yeast multicellularity by an environmentally responsive prion. Cell **153:**153–165. http://dx.doi.org/10.1016/j.cell.2013.02.026.
5. **Lipke PN, Garcia MC, Alsteens D, Ramsook CB, Klotz SA, Dufrêne YF.** 2012. Strengthening relationships: amyloids create adhesion nanodomains in yeasts. Trends Microbiol **20:**59–65. http://dx.doi.org/10.1016/j.tim.2011.10.002.
6. **Dueholm MS, Larsen P, Finster K, Stenvang MR, Christiansen G, Vad BS, Bøggild A, Otzen DE, Nielsen PH.** 2015. The tubular sheaths encasing *Methanosaeta thermophila* filaments are functional amyloids. J Biol Chem. http://dx.doi.org/10.1074/jbc.M115.654780
7. **Shewmaker F, McGlinchey RP, Wickner RB.** 2011. Structural insights into functional and pathological amyloid. J Biol Chem **286:**16533–16540. http://dx.doi.org/10.1074/jbc.R111.227108.
8. **Sawaya MR, Sambashivan S, Nelson R, Ivanova MI, Sievers SA, Apostol MI, Thompson MJ, Balbirnie M, Wiltzius JJ, McFarlane HT, Madsen AØ, Riekel C, Eisenberg D.** 2007. Atomic structures of amyloid cross-beta spines reveal varied steric zippers. Nature **447:**453–457. http://dx.doi.org/10.1038/nature05695.
9. **van Dijk G, van Heijningen S, Reijne AC, Nyakas C, van der Zee EA, Eisel UL.** 2015. Integrative neurobiology of metabolic diseases, neuroinflammation, and neurodegeneration. Front Neurosci **9:**173. http://dx.doi.org/10.3389/fnins.2015.00173.
10. **Hölscher C.** 2014. New drug treatments show neuroprotective effects in Alzheimer's and Parkinson's diseases. Neural Regen Res **9:**1870–1873. http://dx.doi.org/10.4103/1673-5374.145342.
11. **Watt B, van Niel G, Raposo G, Marks MS.** 2013. PMEL: a pigment cell-specific model for functional amyloid formation. Pigment Cell Melanoma Res **26:**300–315. http://dx.doi.org/10.1111/pcmr.12067.
12. **Evans ML, Chapman MR.** 2014. Curli biogenesis: order out of disorder. Biochim Biophys Acta **1843:**1551–1558. http://dx.doi.org/10.1016/j.bbamcr.2013.09.010.
13. **Lipke PN, Ramsook C, Garcia-Sherman MC, Jackson DN, Chan CXJ,**

Bois M, Klotz SA. 2014. Between amyloids and aggregation lies a connection with strength and adhesion. New J Sci **2014:**815102. http://dx.doi.org/10.1155/2014/815102.
14. **Romero D, Aguilar C, Losick R, Kolter R**. 2010. Amyloid fibers provide structural integrity to *Bacillus subtilis* biofilms. Proc Natl Acad Sci U S A **107:**2230–2234. http://dx.doi.org/10.1073/pnas.0910560107.
15. **Serra DO, Richter AM, Klauck G, Mika F, Hengge R**. 2013. Microanatomy at cellular resolution and spatial order of physiological differentiation in a bacterial biofilm. mBio **4:**e00103-13. http://dx.doi.org/10.1128/mBio.00103-13.
16. **Dufrêne YF**. 2015. Sticky microbes: forces in microbial cell adhesion. Trends Microbiol **23:**376–382. http://dx.doi.org/10.1016/j.tim.2015.01.011
17. **Dufrene YF**. 2015. Understanding forces in biofilms. Nanomedicine (Lond) **10:**1219–1221. http://dx.doi.org/10.2217/nnm.15.15.
18. **Halfmann R, Lindquist S**. 2010. Epigenetics in the extreme: prions and the inheritance of environmentally acquired traits. Science **330:**629–632. http://dx.doi.org/10.1126/science.1191081.
19. **Wickner RB, Shewmaker FP, Bateman DA, Edskes HK, Gorkovskiy A, Dayani Y, Bezsonov EE**. 2015. Yeast prions: structure, biology, and prion-handling systems. Microbiol Mol Biol Rev **79:**1–17. http://dx.doi.org/10.1128/MMBR.00041-14.
20. **Pham CL, Kwan AH, Sunde M**. 2014. Functional amyloid: widespread in nature, diverse in purpose. Essays Biochem **56:**207–219. http://dx.doi.org/10.1042/bse0560207.
21. **Ren Q, Kwan AH, Sunde M**. 2013. Two forms and two faces, multiple states and multiple uses: properties and applications of the self-assembling fungal hydrophobins. Biopolymers **100:**601–612. http://dx.doi.org/10.1002/bip.22259.
22. **Alsteens D, Garcia MC, Lipke PN, Dufrêne YF**. 2010. Force-induced formation and propagation of adhesion nanodomains in living fungal cells. Proc Natl Acad Sci U S A **107:**20744–20749. http://dx.doi.org/10.1073/pnas.1013893107.
23. **Garcia MC, Lee JT, Ramsook CB, Alsteens D, Dufrêne YF, Lipke PN**. 2011. A role for amyloid in cell aggregation and biofilm formation. PLoS One **6:**e17632. http://dx.doi.org/10.1371/journal.pone.0017632.
24. **Bois M, Singh S, Samlalsingh A, Lipke PN, Garcia MC**. 2013. Does *Candida albicans* Als5p amyloid play a role in commensalism in *Caenorhabditis elegans*? Eukaryot Cell **12:**703–711. http://dx.doi.org/10.1128/EC.00020-13
25. **Gilchrist KB, Garcia MC, Sobonya R, Lipke PN, Klotz SA**. 2012. New features of invasive candidiasis in humans: amyloid formation by fungi and deposition of serum amyloid P component by the host. J Infect Dis **206:**1473–1478. http://dx.doi.org/10.1093/infdis/jis464.
26. **Garcia-Sherman MC, Lundgren T, Sobonya R, Lipke PN, Klotz SA**. 2015. A unique biofilm in human deep mycoses: fungal amyloid is bound by host serum amyloid P component. NPJ Biofilms Microbiomes **1:**15009. http://dx.doi.org/10.1038/npjbiofilms.2015.9.
27. **Garcia-Sherman MC, Lysak N, Filonenko A, Richards H, Sobonya RE, Klotz SA, Lipke PN**. 2014. Peptide detection of fungal functional amyloids in infected tissue. PLoS One **9:**e86067. http://dx.doi.org/10.1371/journal.pone.0086067.
28. **Lin J, Oh SH, Jones R, Garnett JA, Salgado PS, Rusnakova S, Matthews SJ, Hoyer LL, Cota E**. 2014. The peptide-binding cavity is essential for Als3-mediated adhesion of Candida albicans to human cells. J Biol Chem **289:**18401–18412. http://dx.doi.org/10.1074/jbc.M114.547877.
29. **Gaur NK, Klotz SA**. 1997. Expression, cloning, and characterization of a *Candida albicans* gene, *ALA1*, that confers adherence properties upon *Saccharomyces cerevisiae* for extracellular matrix proteins. Infect Immun **65:**5289–5294.
30. **Gaur NK, Klotz SA, Henderson RL**. 1999. Overexpression of the *Candida albicans ALA1* gene in *Saccharomyces cerevisiae* results in aggregation following attachment of yeast cells to extracellular matrix proteins, adherence properties similar to those of *Candida albicans*. Infect Immun **67:**6040–6047.
31. **Kapteyn JC, Hoyer LL, Hecht JE, Müller WH, Andel A, Verkleij AJ, Makarow M, Van Den Ende H, Klis FM**. 2000. The cell wall architecture of *Candida albicans* wild-type cells and cell wall-defective mutants. Mol Microbiol **35:**601–611. http://dx.doi.org/10.1046/j.1365-2958.2000.01729.x.
32. **Dranginis AM, Rauceo JM, Coronado JE, Lipke PN**. 2007. A biochemical guide to yeast adhesins: glycoproteins for social and antisocial occasions. Microbiol Mol Biol Rev **71:**282–294. http://dx.doi.org/10.1128/MMBR.00037-06.
33. **Alsteens D, Beaussart A, Derclaye S, El-Kirat-Chatel S, Park HR, Lipke PN, Dufrene YF**. 2013. Single-cell force spectroscopy of Als-mediated fungal adhesion. Anal Methods **5:**3657–3662. http://dx.doi.org/10.1039/C3AY40473K.
34. **Rauceo JM, Gaur NK, Lee KG, Edwards JE, Klotz SA, Lipke PN**. 2004. Global cell surface conformational shift mediated by a *Candida albicans* adhesin. Infect Immun **72:**4948–4955. http://dx.doi.org/10.1128/IAI.72.9.4948-4955.2004.
35. **Chan CX, Joseph IG, Huang A, Jackson DN, Lipke PN**. 2015. Quantitative analyses of force-induced amyloid formation in *Candida albicans* Als5p: activation by standard laboratory procedures. PLoS One **10:**e0129152. http://dx.doi.org/10.1371/journal.pone.0129152.
36. **Alsteens D, Dupres V, Klotz SA, Gaur NK, Lipke PN, Dufrêne YF**. 2009. Unfolding individual Als5p adhesion proteins on live cells. ACS Nano **3:**1677–1682. http://dx.doi.org/10.1021/nn900078p.
37. **Barten DM, Albright CF**. 2008. Therapeutic strategies for Alzheimer's disease. Mol Neurobiol **37:**171–186. http://dx.doi.org/10.1007/s12035-008-8031-2.
38. **Dai B, Li D, Xi W, Luo F, Zhang X, Zou M, Cao M, Hu J, Wang W, Wei G, Zhang Y, Liu C**. 2015. Tunable assembly of amyloid-forming peptides into nanosheets as a retrovirus carrier. Proc Natl Acad Sci U S A **112:**2996–3001. http://dx.doi.org/10.1073/pnas.1416690112.
39. **Morris KL, Zibaee S, Chen L, Goedert M, Sikorski P, Serpell LC**. 2013. The structure of cross-beta tapes and tubes formed by an octapeptide, alphaSbeta1. Angew Chem Int Ed **52:**2279–2283. http://dx.doi.org/10.1002/anie.201207699.
40. **Fernandez-Escamilla AM, Rousseau F, Schymkowitz J, Serrano L**. 2004. Prediction of sequence-dependent and mutational effects on the aggregation of peptides and proteins. Nat Biotechnol **22:**1302–1306. http://dx.doi.org/10.1038/nbt1012.
41. **Conchillo-Solé O, de Groot NS, Avilés FX, Vendrell J, Daura X, Ventura S**. 2007. AGGRESCAN: a server for the prediction and evaluation of "hot spots" of aggregation in polypeptides. BMC Bioinformatics **8:**. http://dx.doi.org/10.1186/1471-2105-8-65
42. **Chan CX, Lipke PN**. 2014. Role of force-sensitive amyloid-like interactions in fungal catch bonding and biofilms. Eukaryot Cell **13:**1136–1142. http://dx.doi.org/10.1128/EC.00068-14.
43. **Ramsook CB, Tan C, Garcia MC, Fung R, Soybelman G, Henry R, Litewka A, O'Meally S, Otoo HN, Khalaf RA, Dranginis AM, Gaur NK, Klotz SA, Rauceo JM, Jue CK, Lipke PN**. 2010. Yeast cell adhesion molecules have functional amyloid-forming sequences. Eukaryot Cell **9:**393–404. http://dx.doi.org/10.1128/EC.00068-09.
44. **Ladiwala AR, Bhattacharya M, Perchiacca JM, Cao P, Raleigh DP, Abedini A, Schmidt AM, Varkey J, Langen R, Tessier PM**. 2012. Rational design of potent domain antibody inhibitors of amyloid fibril assembly. Proc Natl Acad Sci U S A **109:**19965–19970. http://dx.doi.org/10.1073/pnas.1208797109.
45. **Tessier PM, Lindquist S**. 2007. Prion recognition elements govern nucleation, strain specificity and species barriers. Nature **447:**556–561. http://dx.doi.org/10.1038/nature05848
46. **Ebner A, Wildling L, Kamruzzahan AS, Rankl C, Wruss J, Hahn CD, Hölzl M, Zhu R, Kienberger F, Blaas D, Hinterdorfer P, Gruber HJ**. 2007. A new, simple method for linking of antibodies to atomic force microscopy tips. Bioconjug Chem **18:**1176–1184. http://dx.doi.org/10.1021/bc070030s.
47. **Hoyer LL, Green CB, Oh SH, Zhao X**. 2008. Discovering the secrets of the *Candida albicans* agglutinin-like sequence (*ALS*) gene family—a sticky pursuit. Med Mycol **46:**1–15. http://dx.doi.org/10.1080/13693780701435317.
48. **Salgado PS, Yan R, Taylor JD, Burchell L, Jones R, Hoyer LL, Matthews SJ, Simpson PJ, Cota E**. 2011. Structural basis for the broad specificity to host-cell ligands by the pathogenic fungus *Candida albicans*. Proc Natl Acad Sci U S A **108:**15775–15779. http://dx.doi.org/10.1073/pnas.1103496108.